Pressure dependence of elastic constants and of shear mode instability for Nb_3Sn

Z. P. Chang and G. R. Barsch
Department of Physics and Materials Research Laboratory, The Pennsylvania State University, University Park, Pennsylvania 16802
(Received 23 January 1980)

The pressure dependence of the three single-crystal elastic constants of Nb_3Sn has been measured by means of the ultrasonic pulse superposition method from about 13 to 300 K. The first pressure derivative of the soft shear modulus $\frac{1}{2}(c_{11}-c_{12})$ decreases almost monotonically with decreasing temperature from +1.4 at 300 K to −1 above the structural transformation temperature at 45 K. The pressure coefficient of the critical temperature corresponding to vanishing shear modulus agrees approximately with the pressure coefficient of the structural transformation temperature, which is of opposite sign to that in V_3Si. Above 100 K the Grüneisen parameter calculated from the elastic data in the anisotropic continuum approximation agrees well with the thermal Grüneisen parameter, but below 80 K discrepancies occur which are attributed to precursor effects of the transformation. The temperature variation of the pressure coefficient of the soft shear modulus cannot be explained on the basis of the Labbé-Friedel model even if pressure-induced interband charge transfer is included.

I. INTRODUCTION

The $A15$ compounds Nb_3Sn and V_3Si both have high superconducting transition temperatures T_c (18 and 17 K, respectively[1]), and both exhibit elastic-shear-mode softening associated with a structural transformation from cubic to tetragonal symmetry at a temperature T_L (about 45 and 21 K, respectively[1]). However, the two compounds differ in that for Nb_3Sn the lattice constant ratio c/a in the tetragonal phase is smaller than one, the pressure coefficient of T_c is negative,[2] and the pressure coefficient of T_L is positive,[3] whereas for V_3Si the lattice constant ratio is larger than one, and the pressure coefficients of T_c and T_L have signs opposite[4–6] to Nb_3Sn. Since all these quantities are related to the third-order elastic (TOE) constants these differences should be reflected in the TOE constants and other anharmonic properties. Specifically, it follows from the Born stability condition that the pressure coefficients of the transformation temperature T_L and of the soft shear modulus $c_S=\frac{1}{2}(c_{11}-c_{12})$ near T_L should be of opposite sign.[7] For transforming V_3Si this is indeed the case[7]; however, the pressure coefficient of c_S shows unusual behavior[7] in that it exhibits two changes of sign between T_L and 300 K.

In order to compare the behavior of V_3Si and Nb_3Sn we have measured the pressure derivatives of the three single-crystal elastic constants of transforming Nb_3Sn as a function of temperature. The purpose of the present paper is to report the results and to apply them to a study of the stability limit versus pressure. In addition, the first and second Grüneisen parameters are calculated from the elastic data and compared with the available thermal data.[8] Furthermore, the applicability of the Labbé-Friedel model, earlier found adequate for the pressure coefficient of the soft shear modulus in V_3Si if pressure induced interband charge transfer is included,[9,10] is investigated for Nb_3Sn.

II. EXPERIMENTAL DETAILS

A. Crystal specimen

The single crystal of Nb_3Sn used for the present measurements was kindly supplied by Dr. L. J. Vieland, RCA Laboratories, Princeton. It had been grown by an HCl-gas-transport method[11] and was subsequently annealed for about 50 h at 1000 °C in vacuum. The crystal undergoes the cubic-tetragonal structural transformation[12,13] at about 45 K, and the elastic properties measured at zero pressure are very similar to those reported earlier[14,15] for transforming Nb_3Sn. The density of the sample measured by the liquid immersion method was found to be 8.849 g/cm^3 at 23.20 °C, less than the value of 8.87 g/cm^3 reported before for a similar transforming sample,[15] but larger than that for a nontransforming sample[16] (8.83 g/cm^3).

The Nb_3Sn crystal had the form of a 2.5-mm-thick platelet with (110) faces and lateral dimensions of 3 to 4 mm. The crystal was oriented to within 0.5° by means of the Laue back-reflection method. A pair of parallel (110) faces was prepared and carefully polished with 1-μm diamond paste. A check of the finished surfaces against an optical flat under sodium light showed flatness of better than $\frac{1}{2}\lambda$ over most of the area. Initially the distance between the pair of

(110) faces was 2.4663 mm, but after a corner was chipped off in the course of the measurements the platelet was reground to a thickness of 1.9260 mm. Because of the irregular sample shape the lateral dimensions of one of the (110) faces were about 3 mm, and those of the other face about 4 mm.

B. Elastic-constant measurements

The ultrasonic pulse superposition method[17] with an automatic electronic peak finder[18] was used to measure the transit time of 20-MHz longitudinal and transverse sound waves in the [110] direction, from which the three independent elastic constants c_{11}, c_{12}, and c_{44} can be obtained. The measurements were made as a function of pressure at constant temperature for a number of temperatures between about 13 K and room temperature. For the generation of the longitudinal and transverse waves X and AC cut quartz transducers with diameter of 3.1 mm were used. It was found that in the entire temperature range Nonaq stopcock grease was satisfactory for the coupling of the transducer to the sample.

The room-temperature measurements were made up to 1 GPa (10 kbar) in a conventional pressure vessel. The pressure was measured by means of a Manganin resistance cell with an accuracy of 0.5%. For the low-temperature runs a specially designed beryllium-copper vessel was used, which was screwed onto the controlled-temperature block of a Cryogenic Associates model CT14 cryostat.[19] Helium gas was used as a pressure medium, and pressure was read with a Heise gauge with an accuracy of 3×10^5 Pa. The maximum pressure was limited by the pressure vessel, which had been designed for only 0.2 GPa in order to reduce the heat capacity and facilitate more rapid cooling, and below 20 K by the freezing pressure of helium. Thus at 13 K, for example, the highest pressure attained was only about 0.1 GPa, and between 20 and 300 K a pressure range up to 0.18 GPa was used. Above 30 K the temperature was controlled to about 0.01 K by means of a platinum resistance thermometer, and below 30 K with a germanium resistance thermometer. In order to assess the absolute accuracy of the temperature measurement, in addition to these two resistance thermometers located at one end of the pressure vessel[19] a Lakeshore Cryotronics silicon diode was attached to the other end of the pressure vessel for a control run. From the maximum recorded temperature difference of 0.3 K between the two ends of the pressure vessel it is estimated that the absolute accuracy of the temperature measurement at the sample is better than 0.2 K.

For each low-temperature run the vessel with the sample was first pressurized at room temperature to a pressure somewhat larger than the desired pressure, and then cooled to the temperature desired for the run. Transit-time measurements were made for decreasing pressure. Following each pressure decrement a data point was taken after thermal equilibrium was restored at the particular set temperature of the run.

III. EXPERIMENTAL RESULTS

A. Data analysis

The analysis of the ultrasonic data is carried out in terms of the natural velocity defined by[20] $W = 2l_0/\tau$, where l_0 is the distance between the parallel faces at zero pressure ($\approx$ atmospheric pressure) and at temperature T, referring to a particular run, and τ is the transit time of the ultrasonic wave at pressure p, also at the same temperature T. The interplanar distance l_0 and the density ρ were corrected for thermal expansion by graphical interpolation of the lattice parameter given by Mailfert *et al.*[13] at three temperatures in the cubic phase. These data are compatible with the thermal expansion data of Smith *et al.*[8] For the data analysis in the tetragonal phase the values of l_0 and ρ of the cubic phase immediately above the transformation temperature were used.

Within the scatter of the experimental data the dependence of $\rho_0 W^2$ versus pressure p where ρ_0 denotes the density at zero pressure was found to be linear in the smaller pressure range from 0 to about 0.2 GPa used for the runs below room temperature, but in the pressure range from 0 to 1 GPa used at room temperature a small, but statistically significant nonlinear pressure dependence was found. Consequently, below room temperature the intercept $\rho_0 W_0^2 \equiv (\rho_0 W^2)_{p=0}$ and the slope $(\rho_0 W^2)_0' \equiv (\rho_0 W^2)'_{p=0}$ were determined at each temperature from a least-squares fit of $\rho_0 W^2$ to a linear relation in p, and at room temperature the second pressure derivative $(\rho_0 W^2)_0'' \equiv (\rho_0 W^2)''_{p=0}$ was determined together with $\rho_0 W_0^2$ and $(\rho_0 W^2)_0'$ from a least-squares fit of $\rho_0 W^2$ to a quadratic relation in p.

The isothermal first and second pressure derivatives $c_0' = (\partial c/\partial p)_{p=0}$ and $c_0'' = (\partial^2 c/\partial p^2)_{p=0}$ of the adiabatic effective elastic constant c can then be calculated from[20]

$$c_0' = \rho_0 W_0^2/3B^T + (\rho_0 W^2)_0' \tag{3.1a}$$

and[21]

$$c_0'' = \rho_0 W_0^2 s_0'' + 2(\rho_0 W^2)_0' s_0' + (\rho_0 W^2)_0'' \ . \tag{3.1b}$$

Here B^T denotes the isothermal bulk modulus. The quantities s_0' and s_0'' take into account the pressure-induced dimensional change of the sample and can for cubic symmetry be expressed in terms of the bulk modulus B^T and its isothermal first pressure derivative.[20,21] All quantities in Eq. (3.1) are referred to the temperature of the particular run. Because of the

uncertainty in the thermal-expansion data in the analysis the adiabatic value of bulk modulus was used for B^T in Eq. (3.1).

In the present work the three pure modes propagating in [110] were used, which correspond to polarization in [110], [1$\bar{1}$0], and [001], and for which the effective elastic modulus c is given by $c_L = \frac{1}{2}(c_{11} + c_{12}) + c_{44}$, $c_S = \frac{1}{2}(c_{11} - c_{12})$, and c_{44}, respectively.

B. Second-order elastic constants

In Fig. 1 the zero-pressure values of the effective elastic moduli for the three modes are plotted versus temperature. These results are very similar to those reported previously by Rehwald *et al.*[14–15] for transforming Nb_3Sn.

The shear modulus c_S exhibits the conspicuous softening from a room-temperature value of 6.93×10^{10} to 0.16×10^{10} N/m^2 at 49.5 K. Below this temperature this shear mode could not be observed because of high attenuation. The linearly extrapolated shear modulus becomes zero at 46.8 K, as compared with the 49 K found by Rehwald *et al.*[14,15] This difference, as well as a 2.4% difference in the room-temperature value may probably be attributed mostly to sample differences.

The shear modulus c_{44} decreases monotonically from 300 to 13 K, the lowest temperature of the present measurements. There is a discontinuity, or at least a discontinuity in slope, near 46 K, which may be attributed to the structural transformation. As reported elsewhere,[22] from a study of this mode as a function of pressure, it has been possible to infer a value of 45.2 K for the structural transformation temperature T_L, and a value of the pressure coefficient $(\partial T_L/\partial p) = 2.9$ K/GPa in substantial agreement with the value found by Chu[3] by means of specific-heat and resistivity measurements at high pressure.

The adiabatic longitudinal modulus c_L decreases monotonically from 300 to about 47 K and increases with decreasing T in the tetragonal phase. It should be noted that the data for c_{44} and c_L in the tetragonal phase are averages over the tetragonal domains formed along the three cubic axes.[23]

In Fig. 2 the adiabatic elastic moduli c_{11}^S and c_{12}^S together with the adiabatic bulk modulus $B^S = \frac{1}{3}(c_{11} + 2c_{12})$ calculated from the data of Fig. 1 are shown for the cubic phase. The modulus c_{11}^S decreases, and c_{12}^S increases monotonically from 300 to 47 K. Below 70 K the bulk modulus reaches a constant value of 1.715×10^{11} N/m^2. This value and the room-temperature value of 1.682×10^{11} N/m^2 are, respectively, 6.7 and 10% larger than the corresponding values reported by Rehwald *et al.*[15] Again, the difference may probably be attributed mostly to sample differences, and to some extent to the different ultrasonic methods used. For comparison, the room-temperature value measured on the same sample investigated by Rehwald *et al.*,[15] but prior to annealing and in nontransforming condition[12] is[16] 1.592×10^{11} N/m^2. Unfortunately, the sample used in the present work was too small for measuring the longitudinal mode in [100], which would have allowed an internal consistency check.

It has been suggested by Vieland *et al.*[24] that in the presence of sample inhomogeneities the ultrasonically measured shear modulus c_S close to the structural transition is more representative of the softest part of the crystal, and that the values deduced from a longitudinal modulus in connection with the assumption of constant bulk modulus are more typical of the bulk of the crystal. Consequently, the deduced value of c_S was found to extrapolate to zero at a temperature about 5 K lower than the directly measured

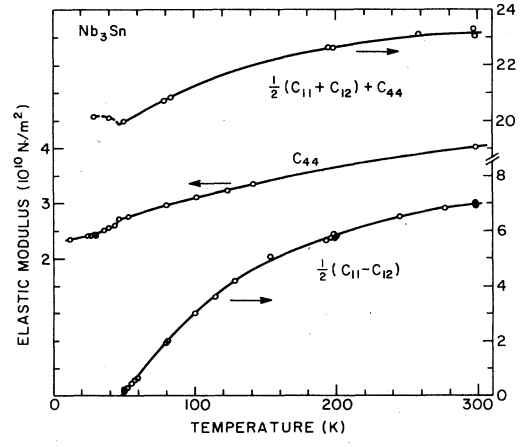

FIG. 1. Effective elastic moduli for the three pure modes in [110] vs temperature.

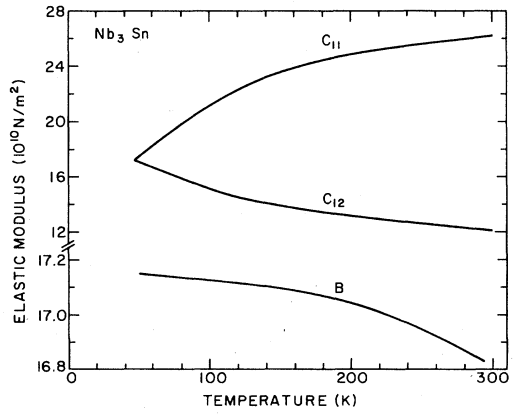

FIG. 2. Adiabatic elastic constants c_{11}^S and c_{12}^S and adiabatic bulk modulus B^S vs temperature (smoothed values).

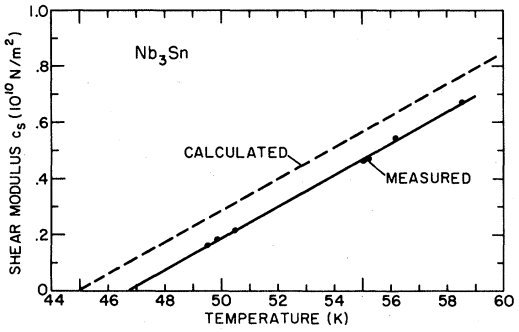

FIG. 3. Comparison of directly measured shear modulus c_S with the value deduced from measured values of c_L and c_{44}, and from $B = 1.712 \times 10^{11}$ N/m^2, assumed to be constant below 100 K (dashed line).

value.[24] Following this procedure we have calculated c_S from the measured values of the longitudinal modulus c_L and the shear modulus c_{44} in conjunction with the assumption of a constant value of 1.712×10^{11} N/m^2 for the bulk modulus below 100 K. The two values of c_S vs T are compared in Fig. 3. At and above 100 K the two curves are identical. It is apparent that the deduced value of c_S extrapolates to zero at 45.0 K. This value is smaller than the structural transformation temperature T_L of 45.2 K for the present sample.[22] Therefore at T_L the shear modulus has a small, but finite value, as required for a weakly first-order phase transition. On the other hand, the temperature at which the directly measured c_S extrapolates to zero is almost 2 K above the value of T_L for the bulk of the sample. This seems to corroborate the above mentioned suggestion of Vieland *et al.*[24] that the deduced value of c_S is more indicative of the bulk properties than the directly measured value. The proximity of the two temperatures at which the deduced and the directly measured values of c_S extrapolate to zero (45.0 and 46.8 K, respectively) may perhaps be taken as an indication that the present sample is more homogeneous than the sample used by Vieland *et al.*,[24] for which these two temperatures differ by 5 K.

C. First pressure derivatives of elastic constants

In Figs. 4(a) and 4(b) the pressure derivatives of the effective elastic moduli for the three modes in [110] as calculated from Eq. (3.1a) are plotted versus temperature. Starting from a room-temperature value of 6.75, between 300 and about 60 K the pressure coefficient $(\partial c_L/\partial p)_T$ for the longitudinal mode decreases by 10% and then drops rather sharply to an almost constant value of 4.0 in the tetragonal phase. Over the same temperature range $(\partial c_{44}/\partial p)_T$ increases by 10% from a value of 1.1 at 300 K and then rises sharply to a weakly temperature-dependent

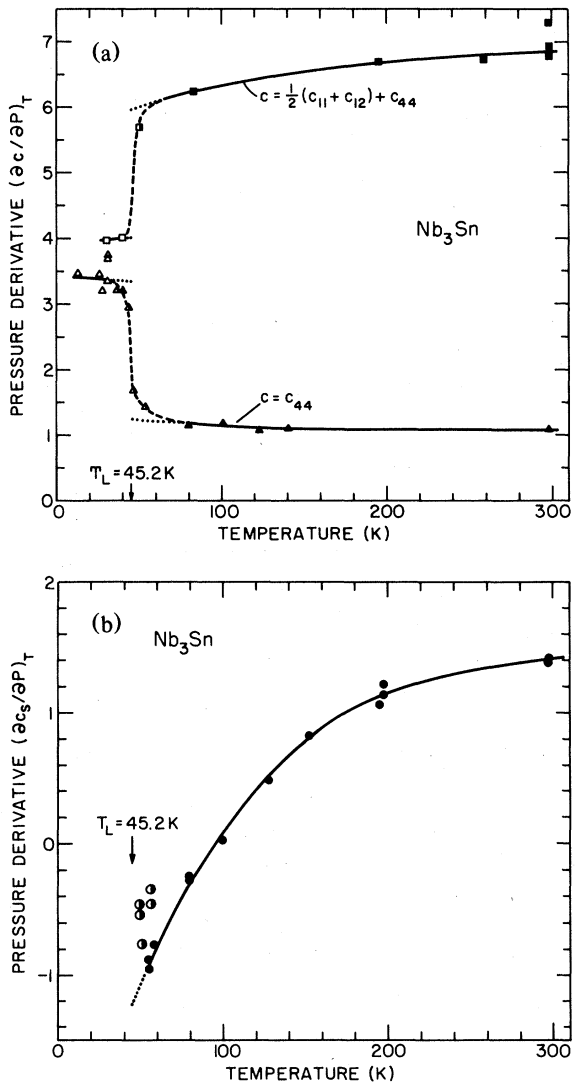

FIG. 4. Isothermal pressure derivatives of the effective elastic moduli for the pure modes measured in [110] vs temperature. Cubic phase: ■, ▲, ●; —— (interpolated); . . . (extrapolated). Tetragonal phase: □, Δ; —— (interpolated); . . . (extrapolated). Precursor and two-phase region: ◨, ◭, ◑; – – – (interpolated). (a) Adiabatic longitudinal modulus c_L and shear modulus c_{44}; (b) shear modulus c_S.

value of about 3.4 in the tetragonal phase. For both modes the largest amount of the change occurs in an interval of about 10 K centered at the structural transition temperature T_L. The near constancy of $(\partial c_{44}/\partial p)_T$ is surprising because c_{44} shows a softening of 33% from 300 K to T_L.

For the pressure coefficient of the soft shear modulus c_S the temperature dependence is quite different. At 300 K its value is +1.4 and depends only weakly on temperature, but with decreasing T it decreases with continuously increasing rate and changes

sign at about 96 K. At 56 K the smallest value of -0.96 is measured. Between 57 and 50 K the curve tends to rise again. However, this rise is attributed to precursor effects of the structural phase transformation because, as will be shown in Sec. IV, the data of the solid curve of Fig. 4(b) and its extrapolation to T_L (indicated by the dotted line) are more compatible with the experimental data of Chu[3] for the pressure dependence of T_L than the data attributed to precursor effects (indicated by half-filled circles). Because of the high ultrasonic attenuation no measurements on this shear mode could be carried out below 50 K.

As for the soft shear modulus, but for reasons discussed below, in the vicinity of T_L the values of $(\partial c_L/\partial p)_T$ and $(\partial c_{44}/\partial p)_T$ pertaining to the pure cubic or tetragonal phase are more likely to be found by extrapolation from the high-temperature cubic-phase or from the low-temperature tetragonal-phase behavior, as shown by the dotted lines in Fig. 4(a). On the other hand, the directly measured data in the transition region from about 35 to 65 K (shown by half-filled symbols) probably indicate precursor effects and (in a smaller temperature interval) the presence of both cubic and tetragonal domains. Precursor effects and a two-phase region have also been observed in x-ray studies.[24]

Figure 5 shows the squared natural velocity ratio $(W/W_0)^2$ versus pressure for the soft shear mode for eight different runs, where W_0^2 is the intercept of the W^2 vs p plot. It indicates the drastic change in slope with temperature displayed in Fig. 4(b). It should be noted, however, that the slopes at lower temperatures are grossly enlarged since W_0^2 in the denominator becomes very small. Figure 5 illustrates the number of data points taken at different pressures for constant temperature, and the low scatter of these data. For the three lowest temperatures only the first few data points at low pressure are included in Fig. 5 because of the large negative slope.

The pressure derivatives $(\partial c_{11}^S/\partial p)_T$, $(\partial c_{12}^S/\partial p)_T$, and $(\partial B^S/\partial p)_T$ calculated from the smoothed curves in Figs. 4(a) and 4(b) are shown in Fig. 6. The solid curves in Fig. 6 refer to the cubic phase. The dotted lines were calculated from the data in Figs. 4(a) and 4(b) extrapolated from the cubic phase in the region where precursors of the phase transformation begin to appear. The dashed curves in Fig. 6 were calculated from the actual measured data in the precursor region. It is apparent that from 300 to 80 K the pressure coefficient of the bulk modulus is virtually independent of temperature. Below 80 K the dashed curve shows a conspicuous temperature dependence, but the dotted curve extends the constant behavior of $(\partial B^S/\partial p)_T$ to lower temperature. Since the bulk modulus itself is virtually constant above T_L, and since the volume change associated with the structural transformation is very small[25,26] it is plausible to assume that $(\partial B^S/\partial p)_T$ should also remain constant

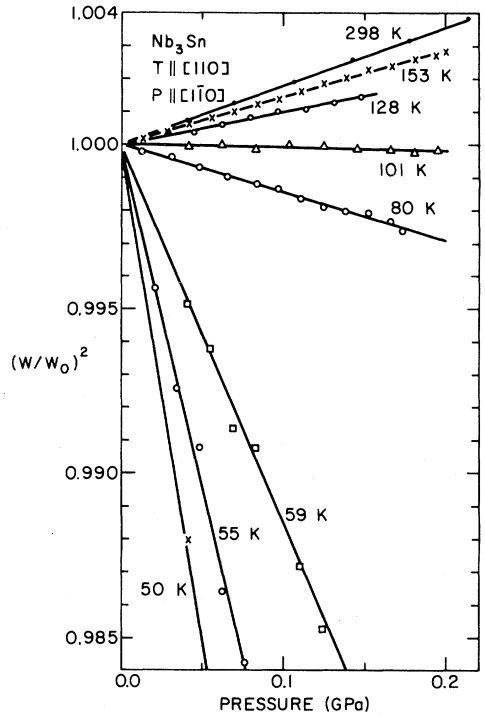

FIG. 5. Squared natural velocity ratio $(W/W_0)^2$ vs pressure for transverse mode in [110] with polarization in [1$\bar{1}$0] for eight selected temperatures.

immediately above T_L. Thus it would follow that the dashed curve in Figs. 6 and 4(a) do not refer to the pure cubic phase, but are affected by the presence of precursor phenomena.

Since the soft shear mode could not be measured below 50 K, and since the crystal available was too small for the measurement of modes other than those in [110] it is not possible to determine the pressure derivatives of the individual single-crystal

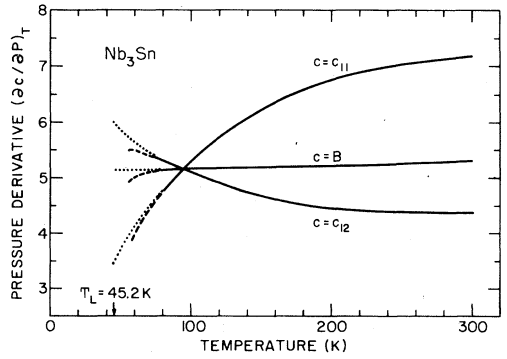

FIG. 6. Isothermal pressure derivatives of adiabatic elastic constants vs temperature: —— from interpolated cubic-phase data; – – – from interpolated precursor data; · · · · from data extrapolated from cubic phase.

elastic moduli in the tetragonal phase from the two measured derivatives $(\partial c_L/\partial p)_T$ and $(\partial c_{44}/\partial p)_T$. Moreover, these two quantities represent averages over the different orientations of the domains in the tetragonal phase.[23] Actually, according to the model calculations of Rehwald *et al.*[15] the second-order elastic moduli in the tetragonal phase of Nb_3Sn do not differ greatly from the conditions for cubic symmetry, viz., $c_{11}=c_{33}$, $c_{12}=c_{23}$, and from the moduli deduced from the measured data in conjunction with the assumption that the bulk modulus remains constant through the phase transformation. However, as will be shown in the following, for the corresponding pressure derivatives much larger deviations from the conditions for cubic symmetry and from the measured data may be expected in the tetragonal phase. Assuming, for example, that the values of $(\partial B/\partial p)_T$ in the cubic and in the tetragonal phase are approximately equal one obtains from the measured values of $(\partial c_L/\partial p)_T$ and $(\partial c_{44}/\partial p)_T$ a large negative average value of $(\partial c_S/\partial p)_T=-13.8$, and average values of $(\partial c_{11}/\partial p)_T=-13.8$ and $(\partial c_{12}/\partial p)_T=+14.3$ in the tetragonal phase. These values are unlikely since they would imply negative thermal expansion, and a positive pressure coefficient $(\partial T_c/\partial p)$ of the superconducting transition temperature in the tetragonal phase, contrary to the experimental facts.[2,8] On the other hand, assuming a positive value of $(\partial c_S/\partial p)_T$ in the tetragonal phase, as suggested by the rise associated with the precursor phenomena in Fig. 4(b) and as would be compatible with the thermal expansion data and the negative value of $(\partial T_c/\partial p)$, a value of $(\partial B/\partial p)_T$ smaller than 0.55 would follow from the values of $(\partial c_L/\partial p)_T$ and $(\partial c_{44}/\partial p)_T$ in the tetragonal phase. However, a large change of $(\partial B/\partial p)_T$ from a value of 5.3 in the cubic phase to a value of 0.55 in the tetragonal phase is very unlikely. One must therefore conclude that the pressure derivatives of the elastic moduli in the tetragonal phase exhibit larger deviations from the conditions for cubic symmetry than the elastic moduli themselves, and/or that the measured pressure derivatives contain a contribution from domain reorientation under pressure. In order to substantiate these suggestions further measurements on single crystals sufficiently large for velocity measurements along different propagation directions and on uniaxially stressed single-domain crystals without domain-wall motion are necessary.

TABLE I. Elastic moduli (in 10^{10} N/m^2) and their isothermal pressure derivatives (dimensionless) for selected temperatures T (K). $c_S=\frac{1}{2}(c_{11}-c_{12})$; $B^S=\frac{1}{3}(c_{11}+2c_{12})$. Values of c_S shown in parentheses are smoothed values calculated from $c_L=\frac{1}{2}(c_{11}+c_{12})+c_{44}$, c_{44}, and $B=17.12\times10^{10}$ N/m^2. Values of $(\partial c/\partial p)$ shown in parentheses are obtained by extrapolation from pure cubic phase, neglecting precursor effects.

T (K)	c_S	c_{44}	B^S	$\left(\frac{\partial c_S}{\partial p}\right)_T$	$\left(\frac{\partial c_{44}}{\partial p}\right)_T$	$\left(\frac{\partial B^S}{\partial p}\right)_T$
300	6.931 ± 0.003	4.013 ± 0.014	16.82 ± 0.09	1.41 ± 0.03	1.08 ± 0.02	5.30 ± 0.27
250	6.56	3.86	16.95	1.33	1.08	5.26
200	5.85	3.65	17.05	1.15	1.09	5.21
150	4.81	3.40	17.10	0.77	1.10	5.18
100	3.01	3.08	17.12	0.08	1.15	5.13
80	1.97 (2.04)	2.95	17.14	−0.29	1.18	5.12
60	0.76 (0.87)	2.82	17.16	−0.78 (−0.78)	1.31 (1.20)	4.99 (5.13)
50	0.19 (0.27)	2.74	17.15	−0.65 (−1.09)	1.53 (1.23)	4.37 (5.13)
47	0.01 (0.12)	2.71	17.15	(−1.18)	1.68 (1.24)	(5.12)
40		2.56			3.15	
30		2.45			3.35	
20		2.39			3.4	
13		2.37			3.4	

TABLE II. Isothermal second pressure derivatives of elastic moduli at 298 K (in units of 10^{-10} m^2/N).

c	c_L	c_{44}	c_S	c_{11}	c_{12}	B
$(\partial^2 c/\partial p^2)_T$	-7 ± 7	-0.75 ± 0.3	-1 ± 0.8	-7 ± 7	-5 ± 7	-6 ± 7

In Table I the smoothed values of the elastic moduli c_S, c_{44}, and B^S and their isothermal pressure derivatives are compiled for selected temperatures. Included in parentheses are the values of c_S deduced from the assumption $B^S=$ const below 100 K, and the values of $(\partial c/\partial p)_T$ in the cubic phase without precursor effects. For the two shear modes the standard errors shown at 300 K were obtained from a least-squares fit of $\rho_0 W^2$ to a quadratic relation in pressure. For the bulk modulus and its pressure derivative the standard errors were obtained by means of the Gaussian error-propagation law.

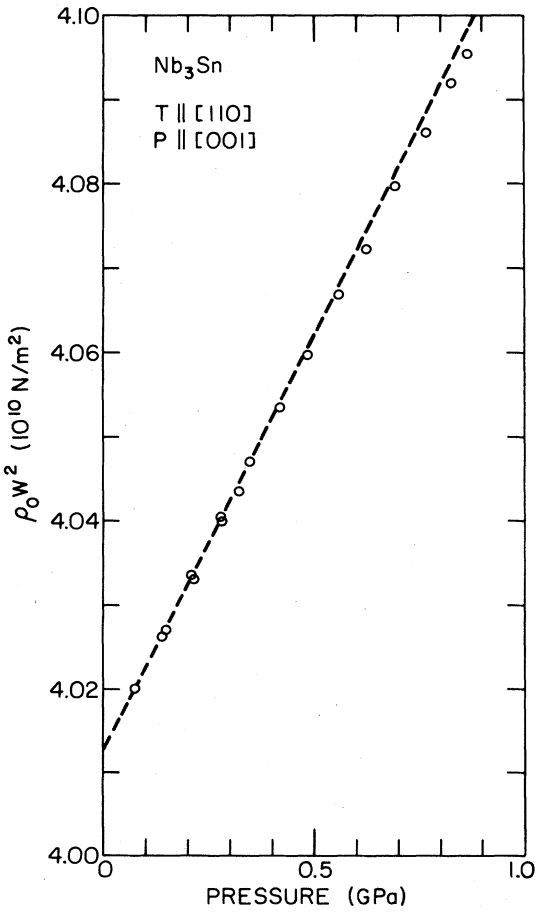

FIG. 7. $\rho_0 W^2$ vs pressure for transverse mode in [110] with polarization in [001] at 298 K. The dashed line indicates the initial tangent at zero pressure.

D. Second pressure derivatives of elastic constants

For the measurements at room temperature a pressure range of about 1 GPa was attained, and a small curvature in the plot of $\rho_0 W^2$ versus pressure was observed for all three modes. For the shear mode associated with the modulus c_{44} the quantity $\rho_0 W^2$ is plotted in Fig. 7 as a function of pressure in order to illustrate the magnitude of the curvature. In Table II the room-temperature values of the second pressure derivatives of the elastic moduli as calculated from Eq. (3.1b) are given. The standard errors for c_L, c_{44}, and c_S were obtained from the least-squares fit of $\rho_0 W^2$ to a quadratic relation in pressure, and those for c_{11}, c_{12}, and B from the Gaussian error-propagation law. For all modes, except c_{44}, the errors are rather large because the data in the $\rho_0 W^2$ vs p plot show larger scatter than in Fig. 7. Hence these data should only be regarded as tentative. For the shear moduli c_{44} and c_S the dimensionless quantities $B(\partial^2 c/\partial p^2)$ are of the same order of magnitude as for alkali halides,[27,28] but for the other moduli they are about ten times larger.

IV. PRESSURE DEPENDENCE OF STABILITY LIMIT

For $A15$ compounds the elastic stability limit[29] is given by the vanishing of the soft shear modulus $c=\frac{1}{2}(c_{11}-c_{12})$ and corresponds to the temperature $T_s=T_s(p)$ below which the cubic phase is mechanically unstable. By expanding $c(T_s,p)=0$ in powers of T_s and p, T_s can be expressed in terms of p. Up to second order, one obtains the truncated expansion

$$T_s=T_s^0+T_s'p+\tfrac{1}{2}T_s''p^2 \ , \tag{4.1}$$

where

$$c(T_s^0,0)=0 \ , \tag{4.2a}$$

$$T_s'=-c_p/c_T \ , \tag{4.2b}$$

$$T_s''=[-c_{pp}(c_T)^2+2c_{pT}c_pc_T-c_{TT}(c_p)^2]/(c_T)^3 \ . \tag{4.2c}$$

The subscripts p and T denote partial derivatives taken at $T_s = T_s^0$ and $p = 0$.

For the numerical application of Eqs. (4.2a) to (4.2c) the value of $T_s^0 = 45$ K as determined from Fig. 3 for the bulk of the crystal, will be used. For the remaining quantities one obtains then from the data in Figs. 3 and 4(b) and in Tables I and II the following values:

$$c_T = (5.9 \pm 0.2) \times 10^8 \text{ N m}^{-2} \text{K}^{-1} , \quad (4.3a)$$

$$c_{TT} = (0 \pm 5) \times 10^6 \text{ N m}^{-2} \text{K}^{-2} , \quad (4.3b)$$

$$c_p = -1.2 \pm 0.2 , \quad (4.3c)$$

$$c_{pp} = (-1 \pm 0.8) \times 10^{-10} \text{ m}^2/\text{N} , \quad (4.3d)$$

$$c_{pT} = (0.029 \pm 0.008) \text{ K}^{-1} . \quad (4.3e)$$

The errors for c_p and c_{pT} are estimates based on the uncertainty arising from extrapolation of c_p as shown by the dotted curve in Fig. 4(b). For c_{pp} and its standard error the room-temperature values have been used. With the above values one obtains

$$T_s' = (2.0 \pm 0.4) \text{ K GPa}^{-1} , \quad (4.4a)$$

$$T_s'' = (-0.03 \pm 0.35) \text{ K GPa}^{-2} . \quad (4.4b)$$

The second pressure derivative of T_s turns out to be zero within experimental error because the first and second term in Eq. (4.2c) almost cancel. The large error of T_s'' arises mostly from the error of c_{pT}.

In Fig. 8 the pressure dependence of the stability limit according to Eqs. (4.1) and (4.4) is compared with the pressure dependence of the structural transformation temperature T_L measured by Chu.[3] For $p > 0.5$ GPa the pressure dependence of T_L is almost linear with a slope of[30] 2.0 K GPa^{-1} in perfect agreement with the slope of T_s' according to Eq. (4.4a). However, below 0.5 GPa the T_L vs p curve rises more steeply. From a fit of Chu's data for T_L to a quadratic relation in p we obtain for the derivatives

$$T_L' = (3.0 \pm 0.2) \text{ K GPa}^{-1} , \quad (4.5a)$$

$$T_L'' = (-0.9 \pm 0.3) \text{ K GPa}^{-2} . \quad (4.5b)$$

Clearly, for both the first and the second derivatives of T_L the discrepancy with the derivatives of T_s is larger than the combined experimental error.

Actually, the pressure dependencies of T_s and T_L need not be exactly the same, because T_s is defined by the vanishing of the soft shear modulus, and T_L by the thermodynamic equilibrium between the cubic and the tetragonal phase. However, because of the nearly second-order character of this phase transformation they should be nearly identical and the discrepancy should be attributed to as yet unaccounted errors in either of the two sets of data.

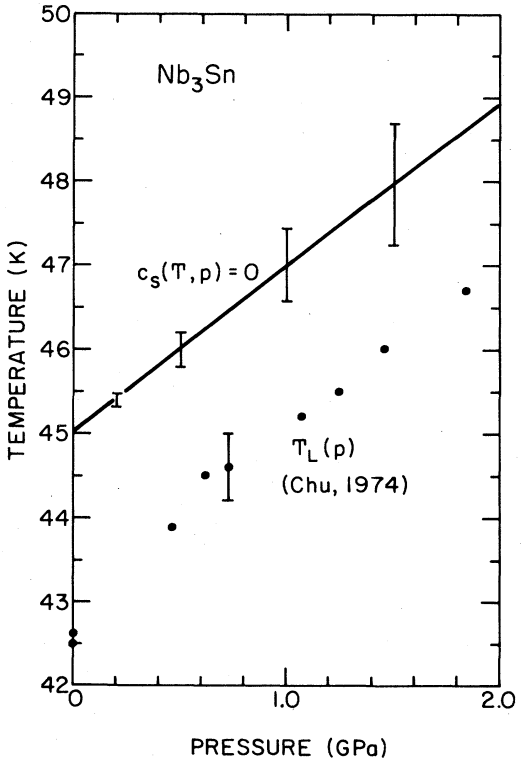

FIG. 8. Comparison of pressure dependence of stability limit, defined by $c_S(T,p) = 0$, with pressure dependence of structural transformation temperature $T_L(p)$ as measured by Chu (Ref. 3). The error bars shown for $c_S(T,p) = 0$ are calculated from the errors of T_s' and T_s'' according to Eqs. (4.4a) and (4.4b).

Although there is no quantitative agreement between the two sets of data their comparison in Fig. 8 shows at least good qualitative agreement. Especially the positive sign of the pressure coefficient of T_L is justified and correlates well with the negative pressure coefficient of the soft shear modulus at T_L^0. Moreover, this comparison provides some justification for the extrapolation of the data for $(\partial c_S/\partial p)$ from the cubic phase as shown by the dotted line in Fig. 4(b) and attributing the half-filled circles in Fig. 4(b) to precursor phenomena. If, on the other hand, the slope T_s' were calculated from these precursor values a much smaller value would result and the discrepancy with T_L' would be increased considerably.

Finally, the difference between the values of $T_s^0 = 45$ K and $T_L^0 = 42.5$ K should be attributed to differences in the samples.[3] The crystal for which $T_L(p)$ was measured by Chu[3] was part of the larger RCA crystal for which $T_L^0 = 43$ K has been measured.[13] The value of $T_L = 45.2$ K measured for the present sample[22] agrees well with the value of 45 K measured on a similar crystal.[24]

V. FIRST AND SECOND GRÜNEISEN PARAMETERS

A. Definitions

The microscopic first and second Grüneisen parameters (mode γ's) are defined in terms of the first and second volume derivatives of the lattice vibrational frequencies according to

$$\gamma_i = -\frac{V}{\omega_i}\left(\frac{\partial \omega_i}{\partial V}\right)_T , \tag{5.1a}$$

$$\gamma_i' = \frac{V^2}{\omega_i}\left(\frac{\partial^2 \omega_i}{\partial V^2}\right) . \tag{5.1b}$$

The macroscopic first (or thermal) Grüneisen parameter defined by

$$\gamma = \frac{\beta B^S}{\rho c_p} \tag{5.2}$$

(β is the volume thermal-expansion coefficient; c_p, the specific heat) is in the quasiharmonic approximation (QHA) given by the mode average[31]

$$\gamma = \sum_i c_i \gamma_i \Big/ \sum_i c_i , \tag{5.3}$$

where c_i denotes the Einstein specific heat of the ith mode.

The three macroscopic second Grüneisen parameters to be considered below are the dimensionless pressure coefficients of the first Grüneisen parameter

$$\gamma^* = B^T\left(\frac{\partial \gamma}{\partial p}\right)_T , \tag{5.4a}$$

the Anderson-Grüneisen parameter[32,33]

$$\delta_S = -\frac{1}{\beta B^S}\left(\frac{\partial B^S}{\partial T}\right)_p , \tag{5.4b}$$

and the parameter introduced by Davis and Parke[34]

$$\xi = \frac{1}{\rho c_v}\left(\frac{\partial B^S}{\partial T}\right)_v \tag{5.4c}$$

(c_v is the specific heat for constant volume). The three second Grüneisen parameters are interrelated through thermodynamic identities according to[35,36]

$$\gamma^* = \{\xi - \gamma[\gamma + 1 + (\partial\gamma/\partial \ln T)_p]\}/R , \tag{5.5a}$$

$$\delta_S = -\frac{\xi}{\gamma R} + \frac{1}{R}\left(\frac{\partial B^S}{\partial p}\right)_T , \tag{5.5b}$$

where $R = B^S/B^T = 1 + \gamma\beta T$. The first term on the right-hand side of Eq. (5.5b) represents the contribution to the temperature coefficient of the bulk modulus at constant volume, and the second term describes the effect of the volume change arising from thermal expansion.

In the QHA the parameter ξ is given by the mode average[37]

$$\xi = \sum_i c_i \gamma_i' \Big/ \sum_i c_i - D , \tag{5.6a}$$

where

$$D = \sum_i \left(\frac{2\epsilon_i}{kT} - 1\right) c_i (\gamma_i - \gamma)^2 \Big/ \sum_i c_i \tag{5.6b}$$

is a weighted mean-square deviation of the first Grüneisen parameter. ϵ_i denotes the energy of the ith mode.

If optic modes and dispersion of acoustic modes are neglected ("anisotropic elastic continuum model") the first and second mode γ's γ_i and γ_i' may be evaluated from the first and second pressure derivatives of the elastic constants, respectively, and the mode averages according to Eqs. (5.3) and (5.6) reduce to directional averages over the propagation directions of the long-wavelength acoustic modes.[38,39,21] Although the anisotropic elastic continuum model is (in the QHA) exact only in the low-temperature limit $T \to 0$, it also often gives good results in the high-temperature limit $T >> \Theta_D$ (Θ_D is the Debye temperature), both for the macroscopic first and second Grüneisen parameters.[39,21] Such behavior might be expected whenever the direction dependence of the mode γ's is larger than their dispersion and their variation among optical and acoustic branches.

B. Results for first Grüneisen parameter

In Figs. 9(a) and 9(b) the three effective elastic constants c_λ and the three elastic mode γ's γ_λ ($\lambda = 1, 2, 3$) are plotted for two temperatures as a function of direction between the three principal symmetry directions. It is apparent that the absolute magnitude of the angular variation is only moderate at 300 K, both for the c_λ and γ_λ, and at 50 K for the c_λ. However, at 50 K because of the shear mode softening the γ_λ for the two transverse modes are strongly direction dependent and show minima of -33 and -5 in [110] and near [111], respectively. In the vicinity of [111] both shear mode γ's are negative. The large negative-mode gammas should give rise to negative thermal expansion below about 50 K in the cubic phase.

In Fig. 10 the thermal Grüneisen parameter γ^{th} from dilatometric measurements on sintered polycrystals by Smith *et al.*[8] is compared with the high- and low-temperature limits ($T >> \Theta_D$ and $T = 0$, respectively) of the elastic Grüneisen parameter γ^{el}, which was evaluated according to Eq. (5.3) by numerical integration over all mode directions. For about $T \gtrsim 100$ K the high- and low-temperature limits agree closely with each other and with the thermal value. However, for $T \lesssim 80$ K both γ_0^{el} and $\gamma_\infty^{\text{el}}$ decrease, and γ^{th} increases sharply with decreasing T.

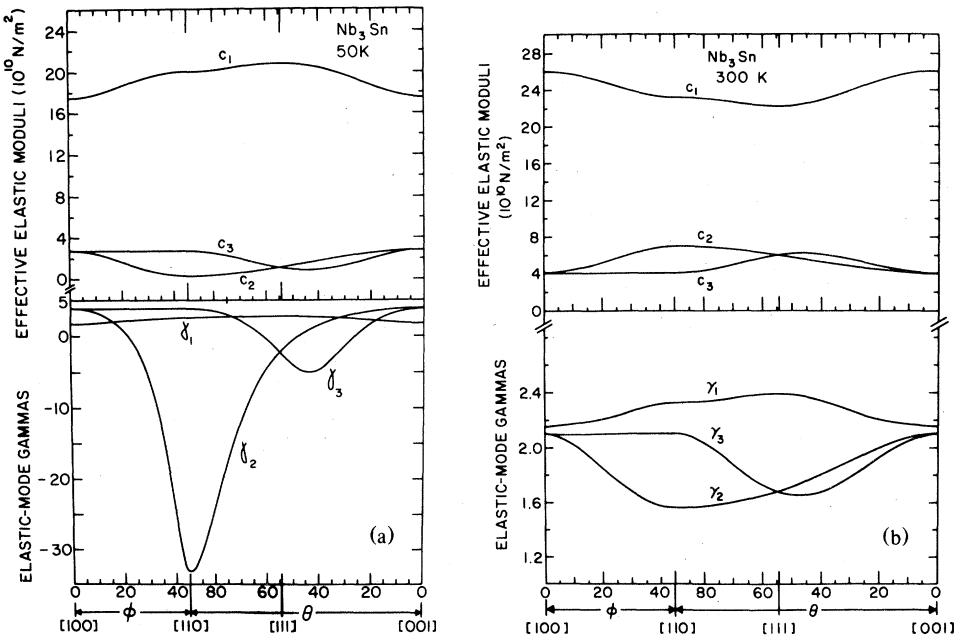

FIG. 9. Orientation dependence of the effective elastic moduli $c_\lambda = \rho_0 W_0^2$ and of the microscopic elastic Grüneisen parameters γ_λ. $\lambda = 1$ denotes the longitudinal mode, $\lambda = 2, 3$ the transverse modes. ϕ and θ are the azimuth and polar angles, respectively. (a) 50 K; (b) 300 K.

The good agreement between γ^{th} and γ^{el} above 100 K suggests that in this temperature range γ^{th} is mostly due to the lattice vibrational contribution and does not include a significant electronic term, and that the dispersion of the mode γ's is less important than their directional dependence. In the following the possible reasons for the discrepancy between γ^{th} and γ^{el} below 80 K are discussed.

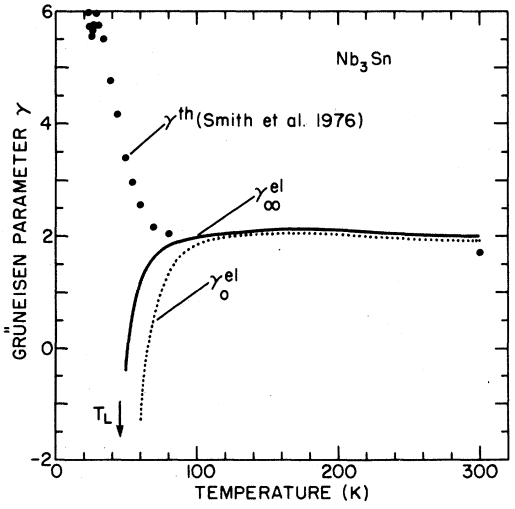

FIG. 10. Thermal Grüneisen parameter γ^{th} (from Smith *et al.*[8]), and low- and high-temperature limits of the elastic Grüneisen parameter γ_0^{el} and γ_∞^{el}, respectively, calculated from ultrasonic elastic data of Table I, vs temperature.

The most obvious cause for this discrepancy, namely, the neglect of dispersion and of the optic modes in γ^{el} is considered unlikely, since it would imply anomalously large positive-mode γ's to overcompensate for the large negative-mode γ's associated with the soft shear mode.

Smith *et al.*[8,40] have suggested that the steep rise in γ^{th} below 80 K could arise from anharmonic or electronic contributions. As for anharmonic effects, the anharmonic contributions not included in the anisotropic continuum approximation have already been discarded above as an unlikely cause, and for the same reason genuine anharmonic contributions not included in the quasiharmonic approximation are not expected to be of major importance either. On the other hand, within the framework of the Labbé-Friedel model[41] the electronic contribution to thermal expansion is negligible as compared with the lattice contribution.[42] It should not be drastically different for the more recent models for the mode softening,[43–45] although this remains to be investigated.

The most likely cause for the steep rise of γ^{th} and for the increasing discrepancy with γ_∞^{el} appears to be precursor effects of the structural transformation between 45 and about 80 K, for the following reasons. First, the rise of γ^{th} below $T_L = 45$ K is associated with the structural transformation. This is evident from observed strain-induced line broadening[8,40] below 45 K and can be inferred from the validity of the Ehrenfest relation $(\partial T_L/\partial p) = V T_L \Delta\beta/\Delta c_p$ relat-

ing the pressure coefficient of T_L with the discontinuities of β and c_p. Second, the negative pressure coefficient of the superconducting transition temperature implies a positive Grüneisen parameter in the tetragonal low-temperature phase.[8,40] Third, if γ^{el} is calculated from the actually measured pressure derivatives of the elastic constants, which include the precursor effects [cf. half-filled symbols in Figs. 4(a) and 4(b)], γ^{el} shows a minimum near 50 K and remains positive at all T, thereby reducing the discrepancy between γ^{th} and γ^{el}.

Precursor effects up to 10 K above the structural transformation in Nb_3Sn occur also in the thermal strain as observed with x-rays.[24] In V_3Si single crystals dilatometric thermal-expansion measurements show precursor strains up to 40 K above the structural transformation temperature of about 20 K.[46,47] The temperature range over which the precursor effects are observed is independent of the residual resistance ratio,[46] but the anisotropy and the sign of the precursor strain is affected by external stress.[47] For V_3Si there appears to be a correlation between these precursor phenomena and d-spacing fluctuations which show up in x-ray line broadening, but not in neutron scattering linewidths, and which have therefore been attributed to effects within a surface layer of the crystal.[48]

Assuming that the precursor effects observed in V_3Si are also indicative of the behavior of Nb_3Sn one may therefore tentatively attribute the discrepancy between γ^{th} and γ^{el} in the cubic phase to the presence of precursor effects in γ^{th}. For a quantitative comparison of γ^{th} and γ^{el} both thermal-expansion and elastic-constant measurements on single crystals in a single-domain state of the tetragonal phase would be required.

C. Results for second Grüneisen parameters

In Table III the room-temperature values of the three second Grüneisen parameters defined in Eqs. (5.4a) to (5.4c) are compared with the values calculated from the elastic data of Tables I and II according to Eqs. (5.5) and (5.6) in the anisotropic continuum approximation and in the high-temperature limit. The elastic values are several times larger than the thermal values, probably because of the large experimental errors of the second pressure derivatives of the elastic constants in Table II. Thus one may conclude from the comparison of the data in Table III that most of the second pressure derivatives in Table II, especially $(\partial^2 c_L/\partial p^2)_T$ and $(\partial^2 B/\partial p^2)_T$, may be several times smaller than reported there. Electronic contributions to δ_S should be small compared with anharmonic contributions.[42]

TABLE III. Comparison of thermal and elastic second Grüneisen parameters for Nb_3Sn. Thermal values are evaluated at 300 K, elastic values refer to the high-temperature limit.

	Thermal	Elastic
γ^*	−8.75	−26.9
δ_S	7.62	15.8
ξ	−4.15	−21.0

From the thermal data in Table III one concludes that the first and the second terms on the right-hand side of Eq. (5.5b) amount to 31 and 69% of δ_S; i.e., the temperature variation of the bulk modulus arises mostly via the thermal-expansion volume effect.

VI. MODEL CALCULATION OF $(\partial c_S/\partial p)_T$

Several theoretical calculations[9,10,49,50] have been made for the temperature dependence of the pressure coefficient $(\partial c_S/\partial p)_T$ of the soft shear modulus of V_3Si. They are based on the linear-chain model of Weger[51] and Labbé and Friedel[41] (WLF) or on the coupled chain model of Gor'kov.[43] The first attempt by Schuster,[49] based on the WLF model, succeeded in explaining the then-available data[52] between 77 and 300 K, but at the expense of using different model parameters for the temperature variation of c_S and $(\partial c_S/\partial p)_T$. Furthermore, Schuster's model could not explain later experimental data of $(\partial c_S/\partial p)_T$ below 77 K for transforming or nontransforming samples.[9,10] The minimum and the second sign reversal of $(\partial c_S/\partial p)_T$ observed[7] in transforming V_3Si below 77 K could be explained by Ting and Ganguli[9] and by Barsch and Rogowski[10] by including pressure-induced interband charge transfer between the d and the s band in the WLF model. However, the qualitatively different behavior and the large negative value of $(\partial c_S/\partial p)_T = -5$ measured[53] at 13.5 K for nontransforming V_3Si could not be explained on the basis of this model.[9,10] While Noolandi and Varma[54] have invoked the effect of defect-induced strains of tetragonal symmetry in order to explain this behavior, Ting[50] has shown that the behavior of both transforming and nontransforming V_3Si can be explained with the Gor'kov density of states (which is equivalent to a special case of the model of Lee *et al.*[44,45]) if different values for the number of d electrons are used for the two types of crystals.

It is the purpose of the present section to show that the experimental $(\partial c_S/\partial p)_T$ vs T data for transforming Nb_3Sn reported in Fig. 4(b) cannot be explained with the WLF density of states in the same manner as for V_3Si, even if interband charge transfer is included.

The parameters which enter the WLF model[42] are the nearest-neighbor (NN) transition-metal (TM) overlap integral $J = 2E_m$ (E_m is the bandwidth of the d band), the Slater parameter q_0 of the d-electron wave functions, the number of electrons Q_d per TM atom in the d band, the NN TM distance a, and the temperature-independent contribution c_S^0 to the soft shear modulus arising from the s electrons. For Nb_3Sn the following values have been proposed[55] for a sample with a transformation temperature of 45 K: $J = 8.7$ eV, $q_0 = 3.4$ nm^{-1}, $Q_d = 0.043$ electrons per Nb atom, $a = 0.268$ nm, and, based on the elastic-constant data of Keller and Hanak,[16] $c_S^0 = 8.49 \times 10^{10}$ N m^{-2}. As the elastic-constant data of Fig. 1 differ somewhat from those of Keller and Hanak[16] we find it necessary to use instead the values $q_0 = 3.47$ nm^{-1} and $c_S^0 = 9.13 \times 10^{10}$ N m^{-2} in order to get a better fit of the c_S vs T data to the theoretical expression of Barisic and Labbé.[42]

In Fig. 11 the experimental values of $(\partial c_S/\partial p)_T$ vs T are compared with theoretical curves calculated from the expression pertaining to the WLF density of states[10] for temperature independent Q_d. Two theoretical curves based on two sets of values for the charge transfer parameter $\beta = -(\partial \ln Q_d/\partial \ln a)_T$ and for $(\partial c_S^0/\partial p)_T$ are shown. For $\beta = 0$ only a weakly temperature-dependent behavior is obtained. For a value of $\beta = 112$ the initial decrease of $(\partial c_S/\partial p)_T$ with decreasing temperature is qualitatively reproduced, but the theoretical curve shows a minimum near 85 K not present in the experimental data. Since for V_3Si the value of β was also found to be positive[10] the sign of β does not correlate with the sign of $(\partial T_L/\partial p)$. By varying the parameters (especially Q_d) a better fit can be obtained for both c_S and $(\partial c_S/\partial p)_T$, but at the expense of worsening the agreement for other experimentally available quantities, especially the lattice constant ratio c/a in the tetragonal phase. Thus the comparison of the theoretical result with the experimental data in Fig. 11 does little more than to demonstrate the probable importance of pressure-induced charge transfer in Nb_3Sn, previously noted[9,10] for V_3Si, and to further illustrate the well-known limitations of the WLF model.[43–45,55]

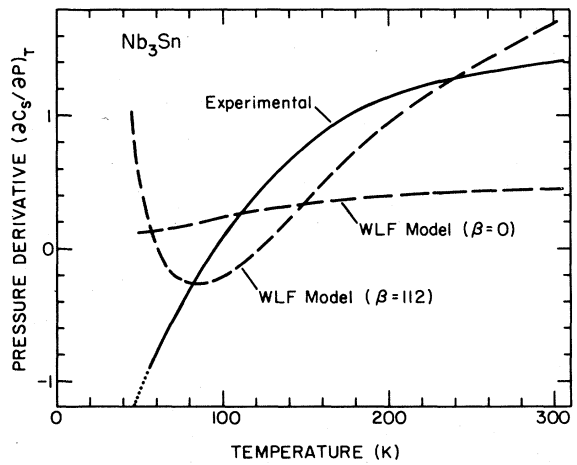

FIG. 11. Comparison of experimental temperature variations of $(\partial c_S/\partial p)_T$ with theoretical results obtained from Labbé-Friedel model without and with pressure-induced interband charge transfer [$\beta = 0$, $(\partial c_S^0/\partial p)_T = 4.67$, and $\beta = 112$, $(\partial c_S^0/\partial p)_T = 0.6$, respectively].

Of the various microscopic models of $A15$ compounds proposed[41,43–46,56–58] the R-point model of Lee *et al.*[44,45] stands out because of its best overall agreement for both Nb_3Sn and V_3Si with the observed temperature variation of the soft shear modulus, of its magnetic field dependence (for V_3Si), and of the magnetic susceptibility. Moreover, first-principles frozen-phonon calculations for Nb_3Ge by Pickett *et al.*[59] qualitatively substantiate the model of Lee *et al.*,[44,45] but indicate a splitting and lowering of the energy levels at both the M and the R point as a result of the optic-mode dimerization of the Nb atoms along a chain direction and could therefore not quantitatively be fitted to this model. Moreover, it has been shown that, at least for V_3Si, a strong enhancement of the electronically driven mode instability may result from anharmonic phonon-phonon interactions.[60] Thus, a comprehensive theory of $A15$ compounds, including the pressure dependence of the soft shear modulus, with band-structure effects and all interactions among electrons and phonons properly included, still remains a challenging task.

VII. SUMMARY AND CONCLUSIONS

The first pressure derivatives of the bulk modulus and of the shear modulus c_{44} of transforming Nb_3Sn were found to be virtually independent of temperature in the cubic phase from 45 to 300 K. However, the first pressure derivative of the soft shear modulus c_S increases with increasing temperature from -1.2 at 45 K to $+1.4$ at 300 K.

The magnitude and the negative sign of $(\partial c_S/\partial p)_T$ at 45 K are consistent with measurements of the pressure dependence of the structural transformation temperature[3] and lead to large negative elastic-mode γ's in [110] and [111]. In the temperature range from about 80 to 300 K the elastic Grüneisen parameter agrees well with the thermal Grüneisen parameter,[8] but below 80 K the elastic Grüneisen parameter decreases, and the thermal Grüneisen parameter increases with decreasing temperature as the structural transformation temperature of 45 K is approached. This discrepancy is attributed mostly to precursor effects of the phase transition which are present in the

thermal-expansion data pertaining to the cubic phase. Such precursor effects are also observed in the pressure coefficients of all three elastic moduli.

For the second pressure derivatives of the elastic moduli estimates are obtained which are very roughly consistent with the thermal values of the second Grüneisen parameters.

Unlike for V_3Si, the strong monotonical temperature variation of $(\partial c_S/\partial p)_T$ cannot be explained on the basis of the WLF density of states with physically plausible values of the parameters, even if pressure induced interband charge transfer is included.

ACKNOWLEDGMENTS

This work was supported by NSF Grant No. DMR 75-03848. We would like to thank Dr. L. J. Vieland for lending the sample of Nb_3Sn. It is a pleasure to acknowledge discussions with Dr. T. K. Lee, Dr. L. R. Testardi, and Dr. S. J. Williamson.

[1]See, for instance, L. R. Testardi, in *Physical Acoustics,* edited by W. P. Mason and R. N. Thurston (Academic, New York, 1973), Vol. 10, p. 193.
[2]C. W. Chu and L. J. Vieland, J. Low Temp. Phys. 17, 25 (1974).
[3]C. W. Chu, Phys. Rev. Lett. 33, 1283 (1974).
[4]S. Huang and C. W. Chu, Phys. Rev. B 10, 4030 (1974).
[5]R. N. Shelton and T. F. Smith, Mater. Res. Bull. 10, 1013 (1975).
[6]C. W. Chu and L. R. Testardi, Phys. Rev. Lett. 32, 766 (1974).
[7]P. F. Carcia and G. R. Barsch, Phys. Status Solidi B 59, 595 (1973).
[8]T. F. Smith, T. R. Finlayson, and A. Taft, Commun. Phys. 1, 167 (1976).
[9]C. S. Ting and A. K. Ganguly, Phys. Rev. B 9, 2781 (1974).
[10]G. R. Barsch and D. A. Rogowski, Mater. Res. Bull. 8, 1459 (1973).
[11]J. J. Hanak and H. S. Berman, J. Phys. Chem. Solids Suppl. 1, 249 (1967).
[12]R. Mailfert, B. W. Batterman, and J. J. Hanak, Phys. Lett. A 24, 315 (1967).
[13]R. Mailfert, B. W. Batterman, and J. J. Hanak, Phys. Status Solidi 32, K67 (1969).
[14]W. Rehwald, Phys. Lett. A 27, 287 (1968).
[15]W. Rehwald, M. Rayl, R. W. Cohen, and G. D. Cody, Phys. Rev. B 6, 363 (1972).
[16]K. R. Keller and J. J. Hanak, Phys. Lett. 21, 263 (1966); Phys. Rev. 154, 628 (1967).
[17]H. J. McSkimin, J. Acoust. Soc. Am. 33, 12, 606 (1961); 37, 864 (1965).
[18]D. L. Miller, Ph.D. thesis (The Pennsylvania State University, University Park, Pa.) (unpublished).
[19]P. F. Carcia and G. R. Barsch, Phys. Rev. B 8, 2505 (1973).
[20]R. N. Thurston and K. Brugger, Phys. Rev. 133, A1604 (1964).
[21]Z. P. Chang and G. R. Barsch, J. Phys. Chem. Solids 32, 27 (1971).
[22]G. R. Barsch, Z. P. Chang, and L. J. Vieland (unpublished).
[23]J. Wanagel and B. W. Batterman, J. Appl. Phys. 41, 3610 (1970).
[24]L. J. Vieland, R. W. Cohen, and W. Rehwald, Phys. Rev. Lett. 26, 373 (1971).
[25]L. J. Vieland, J. Phys. Chem. Solids 31, 1449 (1970).
[26]H. W. King, F. H. Cocks, and J. T. A. Pollock, Phys. Lett. A 26, 77 (1967).
[27]Z. P. Chang and G. R. Barsch, Phys. Rev. Lett. 19, 1381 (1967).
[28]G. R. Barsch and H. E. Shull, Phys. Status Solidi 43, 637 (1971).
[29]M. Born, J. Chem. Phys. 7, 591 (1939).
[30]The slope of 2.0 K GPa^{-1} is determined graphically from Fig. 2 of Ref. 3, but a value of 2.8 K GPa^{-1} is actually reported there.
[31]J. C. Slater, *Introduction to Chemical Physics* (McGraw-Hill, New York, 1939).
[32]E. Grüneisen, Ann. Phys. (Berlin) 39, 257 (1912).
[33]O. L. Anderson, J. Geophys. Res. 72, 3661 (1967).
[34]R. O. Davies and S. Parke, Philos. Mag. 4, 341 (1959).
[35]J. S. Yu, Appl. Sci. Res. 19, 220 (1968).
[36]W. A. Bassett, T. Takahashi, H. K. Mao, and J. S. Weaver, J. Appl. Phys. 39, 319 (1968).
[37]G. R. Barsch and B. N. N. Achar, in *Thermal Expansion - 1971,* edited by M. G. Graham and H. E. Hagy (AIP, New York, 1972), p. 211.
[38]D. E. Schuele and C. S. Smith, J. Phys. Chem. Solids 25, 801 (1964).
[39]K. Brugger and T. Fritz, Phys. Rev. 157, 524 (1967).
[40]T. F. Smith and T. R. Finlayson, in *High-Pressure and Low-Pressure Physics,* edited by C. W. Chu and J. A. Woolam (Plenum, New York, 1978), p. 315.
[41]J. Labbé and J. Friedel, J. Phys. (Paris) 27, 153, 303 (1966).
[42]S. Barisic and J. Labbé, J. Phys. Chem. Solids 28, 2477 (1967).
[43]L. P. Gor'kov, Pis'ma Zh. Eksp. Teor. Fiz. 17, 525 (1973) [JETP. Lett. 17, 379 (1973)]; and Zh. Eksp. Teor. Fiz. 65, 1658 (1973) [Sov. Phys. JETP 38, 830 (1974)].
[44]T. K. Lee, J. L. Birman, and S. J. Williamson, Phys. Rev. Lett. 39, 839 (1977); and Phys. Lett. A 64, 89 (1977).
[45]T. K. Lee and J. L. Birman, Phys. Rev. B 17, 4931 (1978).
[46]M. Milewits and S. J. Williamson, J. Phys. (Paris) Colloq. 39, C6-408 (1978).
[47]T. Fukase, T. Kobayashi, M. Isino, and Y. Muto, J. Phys. (Paris) Colloq. 39, C6-406 (1978).
[48]J. B. Hastings, G. Shirane, and S. J. Williamson, Phys. Rev. Lett. 43, 1249 (1979).
[49]H. Schuster, J. Low Temp. Phys. 8, 93 (1972).
[50]C. S. Ting, in *High-Pressure and Low-Temperature Physics,* edited by C. W. Chu and J. A. Woolam (Plenum, New York, 1978), p. 381.
[51]M. Weger, Rev. Mod. Phys. 36, 175 (1964).
[52]P. F. Carcia, G. R. Barsch, and L. R. Testardi, Phys. Rev. Lett. 27, 944 (1971).

[53]R. E. Larsen and A. L. Ruoff, J. Appl. Phys. 44, 1021 (1973).
[54]J. Noolandi and C. M. Varma, Phys. Rev. B 11, 4743 (1975).
[55]J. Labbé, Phys. Rev. 172, 451 (1968).
[56]M. Weger and I. B. Goldberg, in *Solid State Physics,* edited by H. Ehrenreich, F. Seitz, and D. Turnbull (Academic, New York, 1973), Vol. 28, p. 1.
[57]R. W. Cohen, G. D. Cody, and J. J. Halloran, Phys. Rev. Lett. 19, 840 (1967).
[58]R. N. Bhatt, Phys. Rev. B 16, 1915 (1977).
[59]W. E. Pickett, K. M. Ho, and M. L. Cohen, Phys. Rev. B 19, 1734 (1979).
[60]B. N. N. Achar and G. R. Barsch, Phys. Rev. B 19, 3761 (1979).